nature communications

Article

https://doi.org/10.1038/s41467-024-53093-9

# ASI-RIM neuronal axis regulates systemic mitochondrial stress response via TGF-β signaling cascade

Received: 16 February 2024

Accepted: 30 September 2024

Published online: 19 October 2024

Check for updates

Zihao Wang[1,2,3], Qian Zhang[1,3], Yayun Jiang[1,2], Jun Zhou[1,2] & Ye Tian[1,2]

Morphogens play a critical role in coordinating stress adaptation and aging across tissues, yet their involvement in neuronal mitochondrial stress responses and systemic effects remains unclear. In this study, we reveal that the transforming growth factor beta (TGF-β) DAF-7 is pivotal in mediating the intestinal mitochondrial unfolded protein response ($UPR^{mt}$) in *Caenorhabditis elegans* under neuronal mitochondrial stress. Two ASI sensory neurons produce DAF-7, which targets DAF-1/TGF-β receptors on RIM interneurons to orchestrate a systemic $UPR^{mt}$ response. Remarkably, inducing mitochondrial stress specifically in ASI neurons activates intestinal $UPR^{mt}$, extends lifespan, enhances pathogen resistance, and reduces both brood size and body fat levels. Furthermore, dopamine positively regulates this $UPR^{mt}$ activation, while GABA acts as a systemic suppressor. This study uncovers the intricate mechanisms of systemic mitochondrial stress regulation, emphasizing the vital role of TGF-β in metabolic adaptations that are crucial for organismal fitness and aging during neuronal mitochondrial stress.

The nervous system serves as a central regulatory hub, detecting both environmental and internal stress stimuli, orchestrating a spectrum of physiological processes, and influencing non-autonomous functions such as foraging behavior, immune responses, body fat storage, systemic stress adaptions, and aging[1,2]. Disruptions in mitochondrial function significantly affect neuronal activities and can extend their impact to peripheral tissues, yet the mechanisms by which neuronal circuits transmit mitochondrial stress signals to these tissues remain largely unclear.

In *Caenorhabditis elegans*, various neuronal-specific stressors have been identified that elicit cell non-autonomous responses in peripheral tissues. For instance, knocking down the mitochondrial electron transport chain (ETC) component *cco-1* in neurons activates the mitochondrial unfolded protein response ($UPR^{mt}$) in the intestine, extending lifespan[3]. Similarly, neuronal expression of YFP with a polyglutamine tract (Q40::YFP), disruption of the mitochondrial dynamic regulator FZO-1, or induction of mitochondrial ROS production within neurons can have cell non-autonomous effects in peripheral tissues[4–7]. Additionally, exposure to pathogens bacterial source odorant, 2,3-pentanedione, can induce cell non-autonomous the $UPR^{mt}$ in a serotonin dependent manner[8]. Interestingly, this neuronal coordination of the mitochondrial systemic stress response is not limited to *C. elegans*. For example, in mice, heterodeficiency of the mitoribosomal protein Crif1 in hypothalamic proopiomelanocortin (POMC) neurons activate the mitochondrial stress response in distal adipose tissues, protecting obese mice and improving glucose metabolism[9]. Similarly, genetic inactivation of OPA1, a mitochondrial cristae-remodeling protein, in POMC neurons reduces white adipose tissue (WAT) lipolysis, leading to obesity[10].

Recent studies have identified secreted "mitokine" signals released from neurons experiencing mitochondrial dysfunction that elicit cell non-autonomous effects. These "mitokine" signals include the morphogen Wnt/EGL-20, neurotransmitters like serotonin, and various neuropeptides[4,5,11,12]. The recognition of Wnt as a "mitokine" signal has prompted speculation about the broader role of morphogens in inter-tissue stress communication.

[1]State Key Laboratory of Molecular Developmental Biology, Institute of Genetics and Developmental Biology, Chinese Academy of Sciences, 100101 Beijing, China. [2]University of Chinese Academy of Sciences, 100093 Beijing, China. [3]These authors contributed equally: Zihao Wang, Qian Zhang.
e-mail: ytian@genetics.ac.cn

Wnt and transforming growth factor beta (TGF-β) are crucial morphogens with conserved functions in metazoan. TGF-β extensively cross-talks with the Wnt pathway in various biological contexts, including epithelial-mesenchymal transition, bone formation and remodeling, enterocyte differentiation, cardiac fibrogenesis, and colorectal cancer[13–17]. In *C. elegans*, neuronal TGF-β signaling regulates development[18], food intake[19], pathogen avoidance[20,21], fat metabolism[22], post-prandial quiescence[23], and food-leaving behavior[24]. While Wnt signaling has been implicated in inter-tissue mitochondrial stress communication, the role of TGF-β signaling in orchestrating cell non-autonomous mitochondrial stress responses and influencing systemic metabolic states remains elusive.

To further understand how morphogens participate in the neuronal coordination of systemic mitochondrial stress response, we demonstrate that DAF-7, a TGF-β ligand, secreted from ASI sensory neurons, acts on DAF-1, a TGF-β receptor expressed on RIM interneurons, to coordinate the systemic UPR$^{mt}$ activation. Combining genetic and cell biology approaches, we found that ASI-specific mitochondrial stress is sufficient to induce UPR$^{mt}$ activation in the intestine, leading to extended lifespan and increased pathogen resistance. Notably, this ASI-RIM-mediated UPR$^{mt}$ activation is positively regulated by dopamine but negatively regulated by GABA. Our study establishes a direct link between neuronal mitochondrial stress and systemic stress adaption and longevity via the TGF-β/DAF-7 signaling pathway, highlighting the critical role of neuronal coordination in systemic metabolic adaptations and aging for organismal fitness.

## Results

### TGF-β/DAF-7 is required for the induction of the cell non-autonomous UPR$^{mt}$

To investigate the involvement of TGF-β signaling in cell non-autonomous UPR$^{mt}$ activation, we utilized a UPR$^{mt}$ reporter strain (*hsp-6p::gfp*) in *C. elegans* lacking TGF-β ligands, under neuronal mitochondrial stress induced by either neuronal *cco-1* knockdown or neuronal Q40::YFP expression[3,5]. *C. elegans* features two TGF-β superfamily signaling pathways, each comprising distinct ligands, receptors, and Smads. Specifically, *daf-7*, the homolog of human GDF11, encodes the ligand of the TGF-β Dauer pathway[18], while *dbl-1*, the homolog of human BMP5, encodes the ligand for the TGF-β Sma/Mab pathway[25].

We found that the mutation of *daf-7* significantly suppressed the induction of *hsp-6p::gfp* expression in animals with neuronal *cco-1* knockdown or neuronal Q40::YFP expression (Fig. 1a, b and Supplementary Fig. 1a–d). Moreover, overexpression of *daf-7p::daf-7* partially restored *hsp-6p::gfp* expression in *daf-7(e1372)* mutants (Fig. 1a, b and Supplementary Fig. 1c, d).

Consistent with the reporter results, the *daf-7* mutation significantly suppressed endogenous *hsp-6* and *hsp-60* mRNA levels in animals with neuronal *cco-1* knockdown or neuronal Q40::YFP expression compared with wild-type animals (Fig. 1c and Supplementary Fig. 1e). Additionally, previous studies have shown that the cell non-autonomous UPR$^{mt}$ can also be activated by neuronal Wnt/EGL-20 expression[11], ADL-neuronal Gas (*gsa-1*) or Gaq (*egl-30*) activation[12], and the transgenerational effect of neuronal mitochondrial stress (TGW)[26]. Our findings indicate that the cell non-autonomous UPR$^{mt}$ induced by these systems is dependent on *daf-7* (Supplementary Fig. 1f–m), highlighting the general role of *daf-7* in cell non-autonomous UPR$^{mt}$ regulation. Notably, the *daf-7* mutation did not affect the UPR$^{mt}$ induction in worms fed with *cco-1* RNAi, suggesting that *daf-7* is not involved in cell-autonomous UPR$^{mt}$ activation (Supplementary Fig. 1n, o)[3]. In contrast, the *dbl-1* mutation, which abolishes TGF-β Sma/Mab pathway activity, did not suppress UPR$^{mt}$ induction in neuronal Q40::YFP animals (Supplementary Fig. 1p, q). Similarly, the mutation of *sma-6*, the gene encoding the type I receptor specific to the TGF-β Sma/Mab pathway[27], did not affect the *hsp-6p::gfp* expression induced by neuronal *cco-1* knockdown (Supplementary Fig. 1r, s). These results collectively indicate that loss-of-function mutation in *daf-7*, the ligand of the TGF-β Dauer pathway, suppresses systemic UPR$^{mt}$ activation in response to neuronal mitochondrial stress.

Cell non-autonomous stress communication extends beyond mitochondrial dysfunction to encompass endoplasmic reticulum (ER) or cytosolic (Cyt) protein homeostasis. Neuronal expression of the transcription factor *xbp-1s*, the spliced form of XBP-1, induces the unfolded protein response in the ER (UPR$^{ER}$) in the intestine[28,29]. Similarly, expression of the transcription factor *hsf-1* in neurons activates the unfolded protein response in the cytosol (UPR$^{cyt}$) in the intestine[30,31]. Interestingly, we observed that loss of *daf-7* further induced UPR$^{ER}$ in neuronal *xbp-1s* background, and also further induced UPR$^{cyt}$ in the neuronal *hsf-1* expression background (Supplementary Fig. 1t–w). Therefore, *daf-7* is required for the induction of the systemic UPR$^{mt}$ activation in response to neuronal mitochondrial perturbations.

### DAF-7 acts in ASI chemosensory neurons to coordinate the systemic UPR$^{mt}$ activation

Previous studies have indicated that *daf-7* is exclusively expressed in the ASI-ciliated chemosensory neurons[18,32]. However, data from the *C. elegans* Neuronal Gene Expression Map & Network (CeNGEN) show that *daf-7* is expressed in several neurons, including ASI, OLQ, ASG, ADE, AWA, ASJ, and ASK neuron (Supplementary Fig. 1x)[33–35]. To identify the specific neuronal subtype where *daf-7* is essential for UPR$^{mt}$ activation, we knocked down *daf-7* by expressing double-stranded RNA under specific promoters for each neuron pair (Supplementary Fig. 1x)[36–41].

When *daf-7* was specifically knocked down in ASI neurons using the *gpa-4* promoter[36], we observed a strong suppression of intestinal UPR$^{mt}$ activation in animals with neuronal *cco-1* knockdown in the *sid-1* mutant background. The *sid-1* mutation renders the animals defective in extracellular double-stranded RNA uptake, enabling tissue-specific RNAi treatment (Fig. 1d, e)[33]. This suppression was not observed with *daf-7* knockdown in other neurons subtypes, indicating that *daf-7* functions in ASI neurons to mediate the cell non-autonomous UPR$^{mt}$.

To investigate whether *daf-7* expression is affected under neuronal mitochondrial stress, we monitored its expression using the reporter *daf-7p::gfp* (FK181)[20]. First, we confirmed that *daf-7* is primarily expressed in the ASI chemosensory neurons by colocalizing it with an ASI neuron marker (*str-3p::mCherry*) (Fig. 1f). Additionally, we observed that the fluorescence of *daf-7p::gfp* was induced by neuronal *cco-1* knockdown (Fig. 1g, h), which is consistent with the up-regulated endogenous *daf-7* mRNA level (Fig. 1i). These data suggest the TGF-β signaling is activated in ASI neurons in response to neuronal mitochondrial stress.

### The TGF-β/Dauer signaling pathway is required for cell non-autonomous UPR$^{mt}$ activation

DAF-7 is a TGF-β ligand that governs the TGF-β/Dauer pathway in response to environmental cues. Secreted from sensory neurons, DAF-7 binds to the type I and type II receptors, DAF-1 and DAF-4, in target cells, leading to the phosphorylation of the R-Smads DAF-8 and DAF-14. This phosphorylation negatively regulates the Co-Smad DAF-3 and the Sno/Ski factor DAF-5 (Fig. 2a), promoting reproductive growth and blocking dauer entry[22,42–49]. The function of DAF-7 in preventing dauer entry is dependent on DAF-12, a nuclear hormone receptor[50].

To examine the involvement of the entire TGF-β/Dauer signaling pathway in the cell non-autonomous UPR$^{mt}$ regulation, we introduced loss-of-function mutations in downstream signaling components in animals with neuronal *cco-1* knockdown and measured their UPR$^{mt}$ activation. In line with the canonical TGF-β/Dauer signaling pathway, mutations in *daf-1(m40)*, *daf-4(m63)*, *daf-8(e1393)*, and *daf-14(m77)* strongly suppressed intestinal UPR$^{mt}$ activation in animals with

https://doi.org/10.1038/s41467-024-53093-9

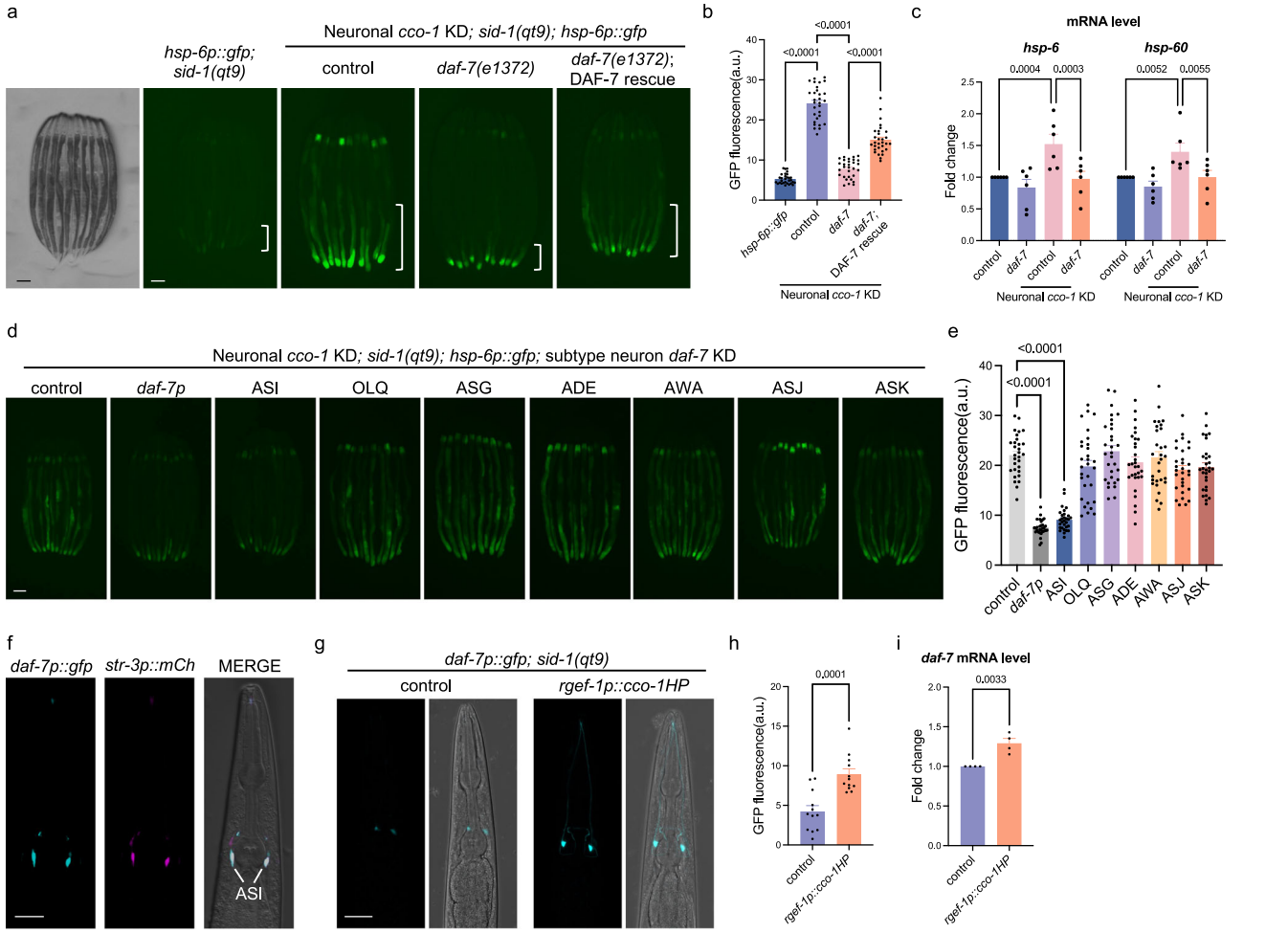


**Fig. 1 | TGF-β/DAF-7 acts in ASI chemosensory neurons to coordinate the cell non-autonomous UPR$^{mt}$.** **a** Representative photomicrographs showing the bright-field images of *hsp-6p::gfp*; and the fluorescence images of *hsp-6p::gfp* in wild type background, neuronal *cco-1* knockdown background, neuronal *cco-1* knockdown and *daf-7* mutation background, neuronal *cco-1* knockdown, *daf-7* mutation and *daf-7p::daf-7*(cDNA) overexpressing background. The posterior region of the intestine where *hsp-6p::gfp* expressed is highlighted. Scale bar, 100 µm. **b** Fluorescence intensities of *hsp-6p::gfp* in animals shown in (**a**) were quantified using ImageJ. n = 30 worms. **c** Relative mRNA levels of *hsp-6* and *hsp-60* in control and *daf-7* mutation with or without neuronal *cco-1* knockdown background. n = 6 biological replicates. **d** Representative fluorescence photomicrographs of *hsp-6p::gfp* in neuronal *cco-1* knockdown background with the expression of *daf-7* dsRNA in indicated sub-type neurons. Scale bar, 100 µm. **e** Fluorescence intensities of *hsp-6p::gfp* in animals shown in (**d**) were quantified using ImageJ. n = 30 worms. **f** Representative fluorescence images of *daf-7p::gfp* (FK181) and *str-3p::mCherry* reporters. Scale bar, 25 µm. **g** Representative fluorescence photomicrographs of *daf-7p::gfp* with or without the expression of *rgef-1p::cco-1 hairpin(HP)*. Scale bar, 25 µm. **h** Fluorescence intensities of *daf-7p::gfp* in ASI neurons of animals shown in (**f**) were quantified using ImageJ. n = 12 neurons. **i** Relative mRNA level of *daf-7* in control and *rgef-1p::cco-1HP* animals. n = 4 biological replicates. *p* values were annotated via two-tailed unpaired *t* test in (**h**) and (**i**), via ordinary one-way ANOVA in (**b**) and (**e**), via two-way ANOVA in (**c**). Error bars, SEM. Source data are provided as a Source Data file. See also Supplementary Fig. 1.

neuronal *cco-1* knockdown or Q40::YFP expression (Fig. 2b, c and Supplementary Fig. 2a, b). Conversely, simultaneous depletion of the negative regulators DAF-3 or DAF-5 in the context of DAF-7 deficiency partially restored UPR$^{mt}$ induction under neuronal mitochondrial stresses (Fig. 2d, e and Supplementary Fig. 2c, d). Notably, *daf-3(e1376)* and *daf-5(e1386)* induced *hsp-6p::gfp* expression in the intestine (Supplementary Fig. 2e, f).

In contrast, the loss of *daf-12* did not restore intestinal UPR$^{mt}$ induction with neuronal *cco-1* knockdown (Fig. 2d, e) or Q40::YFP expression (Supplementary Fig. 2c, d). Thus, while both *daf-3* and *daf-12* are required for dauer entry when *daf-7* is inactivated, suppression of cell non-autonomous UPR$^{mt}$ in these mutants only requires *daf-3*, suggesting a divergence in the molecular mechanisms regulating UPR$^{mt}$ and dauer entry. These findings indicate that the cell non-autonomous UPR$^{mt}$ activation requires the canonical TGF-β Dauer pathway mediated by DAF-7 but is not linked with its role in regulating dauer formation.

## DAF-1 functions in RIM interneurons to mediate cell non-autonomous UPR$^{mt}$

To identify the target cells that receive the DAF-7 signal from ASI neurons and transmit the signal to activate cell non-autonomous UPR$^{mt}$ in the intestine, we focused on DAF-1, the type I receptor of the Dauer pathway[42,43]. Both *daf-1p::gfp* and *daf-1p::daf-1::bfp* reporters showed predominant expression of *daf-1* in the nervous system (Supplementary Fig. 3a). Restoring DAF-1 function using the *daf-1* promoter and the pan-neuronal promoter *rgef-1* in *daf-1(m40)* mutants significantly rescued the suppressed cell non-autonomous UPR$^{mt}$ (Fig. 3a, b and Supplementary Fig. 3b, c). Additionally, pan-neuronal *daf-1* knockdown strongly suppressed intestinal UPR$^{mt}$ activation, confirming the requirement of neuronal DAF-1 for systemic UPR$^{mt}$ activation in response to neuronal mitochondrial stress (Supplementary Fig. 3d, e).

To pinpoint the specific neuronal subset responsible for mediating cell non-autonomous UPR$^{mt}$, we categorized all *daf-1*-expressing

https://doi.org/10.1038/s41467-024-53093-9

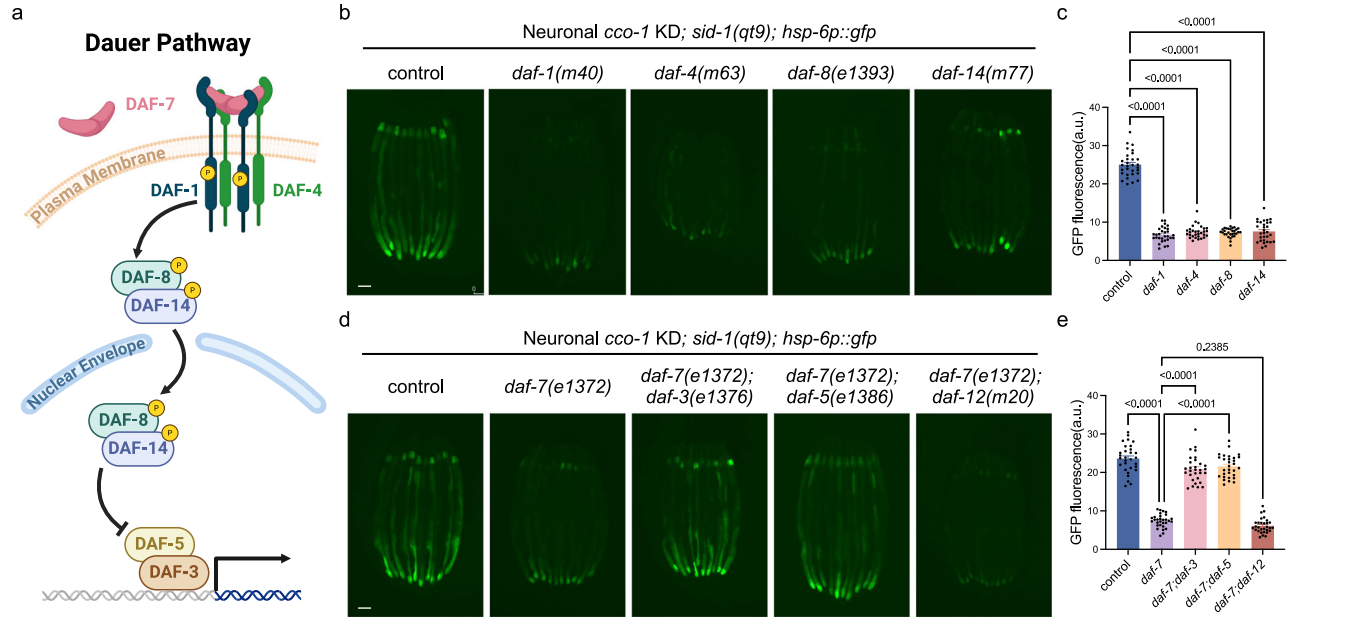


**Fig. 2 | TGF-β/Dauer signaling pathway is required for cell non-autonomous UPR$^{mt}$ activation. a** Schematic diagram of TGF-β/Dauer pathway. Created in BioRender. Wang, Z. (2023) BioRender.com/i90a877. **b** Representative fluorescence photomicrographs of *hsp-6p::gfp* in wild-type, *daf-1, daf-4, daf-8* and *daf-14* animals in neuronal *cco-1* knockdown background. **c** Fluorescence intensities of *hsp-6p::gfp* in animals shown in (**b**) were quantified using ImageJ. n = 30 worms. **d** Representative fluorescence photomicrographs of *hsp-6p::gfp* in wild-type, *daf-7, daf-7;daf-3, daf-7;daf-5* and *daf-7;daf-12* animals in neuronal *cco-1* knockdown background. **e** Fluorescence intensities of *hsp-6p::gfp* in animals shown in (**d**) were quantified using ImageJ. n = 30 worms. *p* values were annotated via ordinary one-way ANOVA in (**c**) and (**e**). Error bars, SEM. Scale bar, 100 μm. Source data are provided as a Source Data file. See also Supplementary Fig. 2.

neurons into seven subsets based on previous studies (Fig. 3c)[51–55]. We then used specific promoters to drive *daf-1* expression in these subsets. Our findings revealed that expressing *daf-1* in set 1 (*tdc-1p::daf-1*) and set 2 (*glr-1p::daf-1*) neurons successfully restored UPR$^{mt}$ induction in *daf-1* mutants with neuronal *cco-1* knockdown (Fig. 3d, e) or neuronal Q40::YFP background (Supplementary Fig. 3f, g). Notably, overexpressing *daf-1* in each set of neurons did not significantly induce *hsp-6p::gfp* expression in the *daf-1(m40)* background, suggesting that overexpression of the receptor alone is not sufficient to induce cell non-autonomous UPR$^{mt}$ (Supplementary Fig. 3h, i). These findings indicate that DAF-1 plays a critical role in RIM interneurons to mediate the cell non-autonomous UPR$^{mt}$.

Next, we selected a RIM-specific expressing promoter, *F23H12.7*, from the *C. elegans* Neuronal Gene Expression Map & Network (CeNGEN) database[33–35], and verified its expression through co-localization analyses with the *tdc-1p::mCherry* reporter, known to express in RIM, RIC, and UV-1 cells (Fig. 3f)[51]. Knocking down *daf-1* in RIM interneurons (*F23H12.7p::dsRNA-daf-1*) strongly suppressed cell non-autonomous UPR$^{mt}$ (Fig. 3g, h). Furthermore, expressing DAF-1 in RIM neurons significantly rescued UPR$^{mt}$ activation in *daf-1(m40)* mutants with neuronal *cco-1* knockdown (Supplementary Fig. 3j, k). Together, these results indicate that DAF-1 functions in RIM interneurons to coordinate the cell non-autonomous UPR$^{mt}$.

## DAF-8 accumulates in the nucleus in response to neuronal mitochondrial stress

To determine if TGF-β signaling is activated in response to pan-neuronal mitochondrial stress, we generated a transgenic strain expressing *daf-8p::daf-8::gfp* to monitor the protein level and subcellular localization of DAF-8, which relocates to the nucleus upon DAF-7 stimulation[56,57]. We specifically labeled RIM neurons using the marker *F23H12.7*p::mCherry, given our previous findings on the role of the receptor DAF-1 in these neurons in responding to neuronal mitochondrial stress. Neuronal *cco-1* knockdown significantly increased the DAF-8 protein level and promoted its nuclear localization, as indicated by higher GFP fluorescence in the nuclei of RIM neurons (Supplementary Fig. 3l). Furthermore, the *daf-7(e1372)* mutation abolished the nuclear accumulation of DAF-8 in RIM neurons of animals with neuronal *cco-1* knockdown (Fig. 3i, j). This finding suggests that the canonical TGF-β Dauer pathway component is activated in response to neuronal mitochondrial stress, leading to a notable nuclear accumulation of TGF-β/DAF-8 Smads in RIM neurons in a DAF-7-dependent manner.

## ASI-specific mitochondrial perturbation is sufficient to activate systemic UPR$^{mt}$ in a *daf-7*-dependent manner

Given the essential role of the ASI-RIM neuron axis in TGF-β signal transduction for cell non-autonomous UPR$^{mt}$ activation, we investigated whether ASI-specific mitochondrial stress alone could drive this process in peripheral tissue. To explore this, we generated transgenic animals with ASI-specific *cco-1* knocked down in the *sid-1(qt9)* mutant background (*gpa-4p::cco-1* HP, referred to as ASI *cco-1* KD). Remarkably, ASI *cco-1* KD significantly induced UPR$^{mt}$ in the intestine, albeit to a lesser extent than pan-neuronal *cco-1* KD, as evidenced by both the *hsp-6p::gfp* reporter and qPCR analyses of endogenous UPR$^{mt}$ target genes (Fig. 4a–c). However, UPR$^{ER}$ and UPR$^{cyt}$ were not activated in ASI *cco-1* KD animals, as accessed by fluorescence reporter (*hsp-4p::gfp and hsp-16.2p::gfp*) (Supplementary Fig. 4a–d) and qPCR analyses (Supplementary Fig. 4e). Furthermore, we generated strains with *cco-1* KD in various neuron subtypes, including ADL, DVB, serotonergic, and GABAergic neurons. We observed that *cco-1* KD in all these neuron types could drive cell non-autonomous UPR$^{mt}$ activation to varying extents, and this effect is also dependent on *daf-7* (Supplementary Fig. 4f–m). These results suggest that mitochondrial stress in different neuron subtypes can induce the cell non-autonomous UPR$^{mt}$, with a common requirement for *daf-7*.

Additionally, *daf-7* expression was elevated in response to ASI *cco-1* KD, as indicated by the transcriptional reporter *daf-7p::gfp* (Fig. 4d, e), and endogenous mRNA levels measured by qPCR (Fig. 4f). Moreover, the intestinal UPR$^{mt}$ activation requires *daf-7* in ASI neurons

https://doi.org/10.1038/s41467-024-53093-9

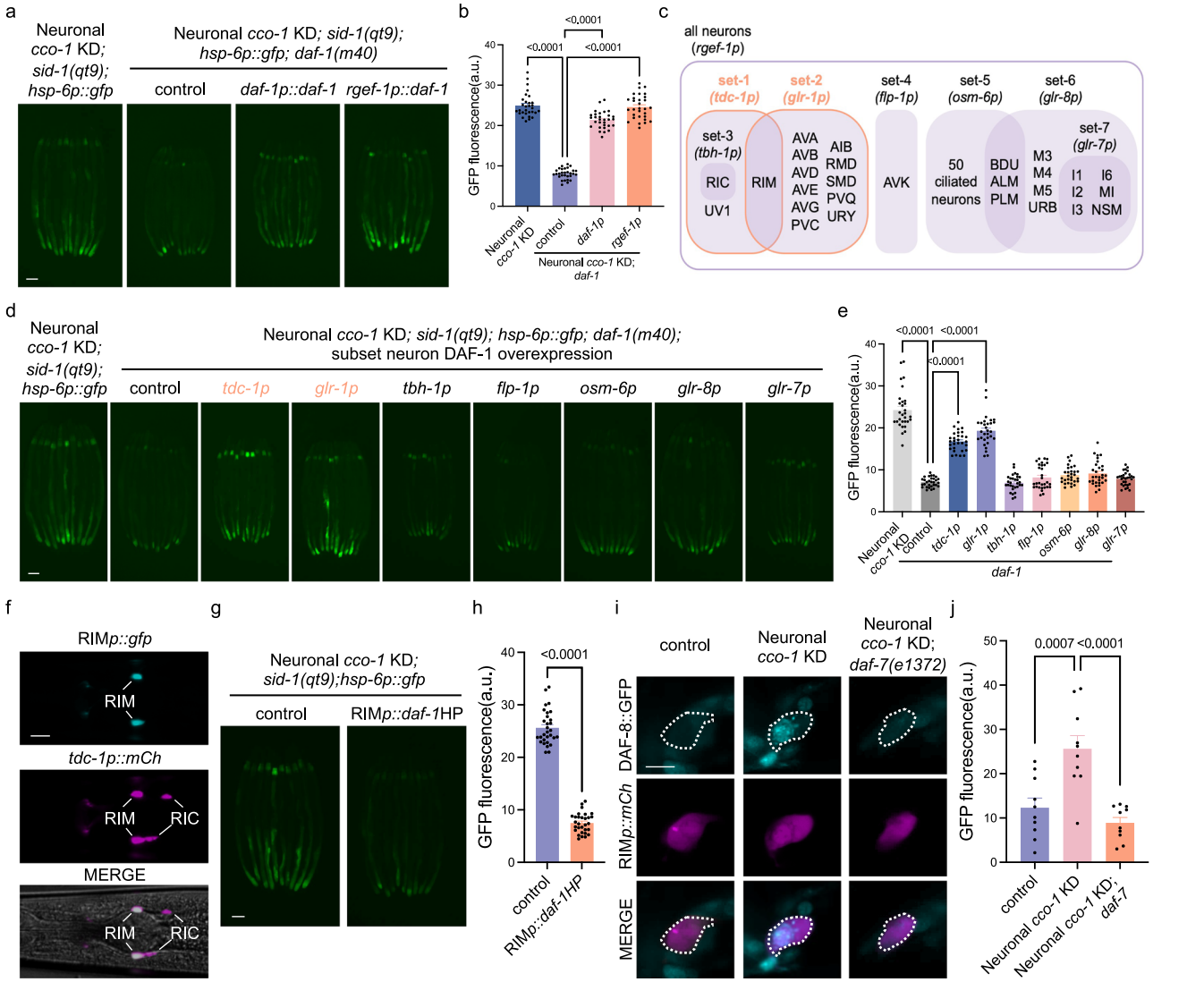


**Fig. 3 | DAF-1 functions in RIM interneurons to mediate cell non-autonomous UPR$^{mt}$.** **a** Representative fluorescence photomicrographs of *hsp-6p::gfp* in wild-type, *daf-1(m40)*, *daf-1(m40);daf-1p::daf-1*, *daf-1(m40);rgef-1p::daf-1*animals in neuronal *cco-1* KD background. Scale bar, 100 µm. **b** Fluorescence intensities of *hsp-6p::gfp* in animals shown in (**a**) were quantified using ImageJ. n = 30 worms. **c** Schematic of subset neurons classification and their specific promoters. **d** Representative fluorescence photomicrographs of *hsp-6p::gfp* in wild-type, *daf-1(m40)* and DAF-1 subtype neurons rescue animals in neuronal *cco-1* KD background. Scale bar, 100 µm. **e** Fluorescence intensities of *hsp-6p::gfp* in animals shown in (**d**) were quantified using ImageJ. n = 30 worms. **f** Representative fluorescence images of head region of animals expressing *F23H12.7p::gfp* (RIM, source from the CeNGEN project) and *tdc-1p::mCherry* (RIM and RIC). Scale bar, 10 µm. **g** Representative fluorescence photomicrographs of *hsp-6p::gfp* in neuronal *cco-1* knockdown background with or without the expression of *F23H12.7p::daf-1 hairpin(HP)*. Scale bar, 100 µm. **h** Fluorescence intensities of *hsp-6p::gfp* in animals shown in (**g**) were quantified using ImageJ. n = 30 worms. **i** Representative fluorescence photomicrographs of *daf-8p::daf-8::gfp; F23H12.7p::mCherry* reporter with or without neuronal *cco-1* knockdown and *daf-7* mutation. Scale bar, 5 µm. **j** Fluorescence intensities of *daf-8p::daf-8::gfp* expression in RIM neurons in animals shown in (**i**) were quantified using ImageJ. n = 10 neurons. *p* values were annotated via two-tailed unpaired *t* test in (**h**), via ordinary one-way ANOVA in (**b**), (**e**) and (**j**). Error bars, SEM. Source data are provided as a Source Data file. See also Supplementary Fig. 3.

and *daf-1* in RIM neurons (Fig. 4g, h). These results suggest that systemic UPR$^{mt}$ activation in response to ASI *cco-1* KD involves the ASI-RIM neuron axis of TGF-β/DAF-7 signaling.

Previous studies have identified several components involved in cell non-autonomous UPR$^{mt}$ activation, including neuropeptides *flp-2*, Wnt ligand *egl-20*, protein disulfide isomerase *pdi-6*, and G-protein-coupled receptor *srz-75*[4,11,12,58–60]. To elucidate their roles in the ASI *cco-1* KD system, we crossed these mutants into ASI *cco-1* KD worms. Surprisingly, none of these mutants significantly suppressed the intestinal UPR$^{mt}$ induced by ASI *cco-1* KD (Supplementary Fig. 4n, o).

To further understand the neuronal coordination network responding to ASI *cco-1* KD, we investigated the involvement of neuronal transmission. The induction of cell non-autonomous UPR$^{mt}$ was significantly reduced in *unc-13* mutants (Fig. 4i, j), a gene essential for the release of small clear vesicles (SCV) and neurotransmitters[61]. In contrast, mutants in *unc-31*, required for the release of dense core vesicles (DCV) containing mainly neuropeptides[62], or *egl-21*, which encodes carboxypeptidase for neuropeptides maturation[63], showed no discernable effect on UPR$^{mt}$ activation in response to ASI *cco-1* KD (Fig. 4i, j). These findings suggest that neurotransmitters are essential for cell non-autonomous UPR$^{mt}$ activation in response to ASI *cco-1* KD.

https://doi.org/10.1038/s41467-024-53093-9

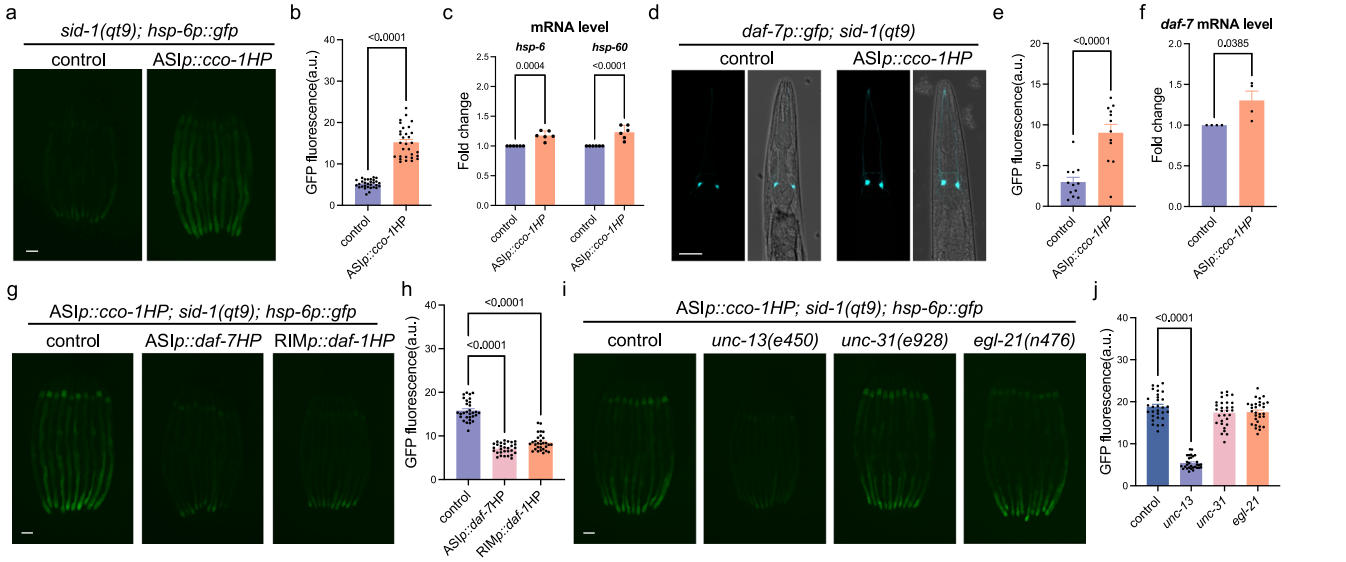


**Fig. 4 | ASI-specific mitochondrial perturbation is sufficient to activate systemic UPR$^{mt}$ in a *daf-7*-dependent manner. a** Representative fluorescence photomicrographs of *hsp-6p::gfp* with or without *gpa-4p::cco-1 hairpin(HP)*. **b** Fluorescence intensities of *hsp-6p::gfp* in animals shown in (**a**) were quantified using ImageJ. n = 30 worms. **c** Relative mRNA levels of *hsp-6* and *hsp-60* in control and *gpa-4p::cco-1HP* animals. n = 3 biological replicates. **d** Representative fluorescence photomicrographs of *daf-7p::gfp* with or without *gpa-4p::cco-1HP*. Scale bar, 25 µm. **e** Fluorescence intensities of *daf-7p::gfp* in ASI neurons of animals shown in (**d**) were quantified using ImageJ. n = 12 neurons. **f** Relative mRNA level of *daf-7* in control and *gpa-4p::cco-1HP* animals. n = 4 biological replicates. **g** Representative fluorescence photomicrographs of *hsp-6p::gfp* in *gpa-4p::cco-1HP* background with or without *gpa-4p::daf-7HP* or *F23H12.7p::daf-7HP*. **h** Fluorescence intensities of *hsp-6p::gfp* in animals shown in (**g**) were quantified using ImageJ. n = 30 worms. **i** Representative fluorescence photomicrographs of *hsp-6p::gfp* in *gpa-4p::cco-1HP* with or without *unc-13, unc-31* or *egl-21* mutations. **j** Fluorescence intensities of *hsp-6p::gfp* in animals shown in (**i**) were quantified using ImageJ. n = 30 worms. *p* values were annotated via two-tailed unpaired *t* test in (**b**), (**e**) and (**f**), via ordinary one-way ANOVA in (**h**) and (**j**), via two-way ANOVA in (**c**). Error bars, SEM. Scale bar, 100 µm. Source data are provided as a Source Data file. See also Supplementary Fig. 4.

## The UPR$^{mt}$ induced by ASI *cco-1* KD requires dopamine and is negatively regulated by GABA

To further elucidate the mechanism behind ASI-specific mitochondrial stress and systemic UPR$^{mt}$ activation, we examined the roles of neurotransmitters by crossing ASI specific *cco-1* KD animals with various neurotransmitter production or packaging mutants. We found that loss of *cat-2*, a gene involved in dopamine synthesis[64], significantly suppressed the UPR$^{mt}$ induced by ASI *cco-1* KD (Fig. 5a, b). Additionally, we investigated the effect of four dopamine receptors (*dop-1, dop-2, dop-3*, and *dop-4*) on UPR$^{mt}$ activation[64,65]. Loss of the D1-like receptor *dop-1* strongly suppressed cell non-autonomous UPR$^{mt}$, while loss of the invertebrate-specific receptor *dop-4* partially suppressed it in ASI *cco-1* KD animals (Fig. 5c, d). These suppressions were restored by overexpressing each receptor in the nervous system (Supplementary Fig. 5a–d), but not in the intestine (Supplementary Fig. 5a–d), suggesting that dopamine functions in neurons to activate systemic UPR$^{mt}$.

Surprisingly, loss of *unc-25*, a gene involved in GABA synthesis, further induced intestinal UPR$^{mt}$ activation in ASI *cco-1* KD animals, suggesting that GABA negatively regulate systemic UPR$^{mt}$ activation (Fig. 5a, b). We confirmed that UPR$^{mt}$ activation in response to ASI *cco-1* KD was also further induced in *unc-47* (GABA vesicular transporter) and *unc-30* (homeodomain transcription factor of UNC-25 and UNC-47) mutants (Fig. 5e, f)[66,67]. Moreover, we examined several ionotropic GABA-gated ion channels (*unc-49, lgc-35*, and *exp-1*) and metabotropic GABA-sensitive G protein-coupled receptors (*gbb-1* and *gbb-2*)[68–71], finding that the mutation of *exp-1* further induced the UPR$^{mt}$ (Fig. 5e, f). Moreover, the UPR$^{mt}$ that is activated by *unc-25* mutants is strongly suppressed by *daf-7* mutation, and partially suppressed by *cat-2* mutation (Supplementary Fig. 5e–h). Additionally, the *cat-2* mutant did not suppress UPR$^{mt}$ induced by pan-neuronal *cco-1* knockdown while the *unc-25* mutant further induced it (Supplementary Fig. 5i, j). These results indicate that systemic UPR$^{mt}$ activation in response to ASI *cco-1* KD requires dopamine but is suppressed by GABA.

## Mitochondrial perturbation in ASI neurons alters various physiological characteristics of animals

To broadly investigate the effects of ASI-specific mitochondrial perturbations (ASI *cco-1* KD), we analyzed several physiological characteristics of the animals. Both ASI *cco-1* KD and pan-neuronal *cco-1* knockdown resulted in a reduced brood size in WT background, but not further reduced in *daf-7* mutant backgrounds (Supplementary Fig. 6a). Additionally, these animals exhibited slightly delayed development and a reduced oxygen consumption rate, which persisted even in *daf-7* mutant backgrounds (Supplementary Fig. 6b, c). However, ASI neuronal *cco-1* KD did not affect the bending rates or crawling ability of these animals (Supplementary Fig. 6d, e).

Next, we explored how ASI-specific mitochondrial perturbations influence systemic metabolic states and longevity. We first assessed lifespan and stress resistance in animals with ASI *cco-1* KD. Mitochondrial perturbation in ASI neurons alone was sufficient to extend lifespan, dependent on *daf-7* in ASI neurons and *daf-1* in RIM neurons (Fig. 6a, b and Supplementary Fig. 6f). Loss of *daf-7* also suppressed the extended lifespan in the pan-neuronal *cco-1* knockdown background (Fig. 6c and Supplementary Fig. 6g). Furthermore, ASI *cco-1* KD animals survived significantly longer than control animals when exposed to the pathogen *Pseudomonas aeruginosa* (PA14), a pathogen that kills *C. elegans* within days of exposure[72,73], which is dependent on *daf-7* in ASI neurons and *daf-1* in RIM neurons (Fig. 6d, e). Loss of *daf-7* similarly suppressed pathogen resistance in the pan-neuronal *cco-1* knockdown background (Fig. 6f). These data confirmed the crucial role of ASI-RIM axis in coordinating cell non-autonomous UPR$^{mt}$, lifespan extension, and pathogen resistance via TGF-β signaling.

ASI neurons in *C. elegans* are known to sense food and nutritional status, regulate lipid metabolism, and modulate endocrine signaling

https://doi.org/10.1038/s41467-024-53093-9

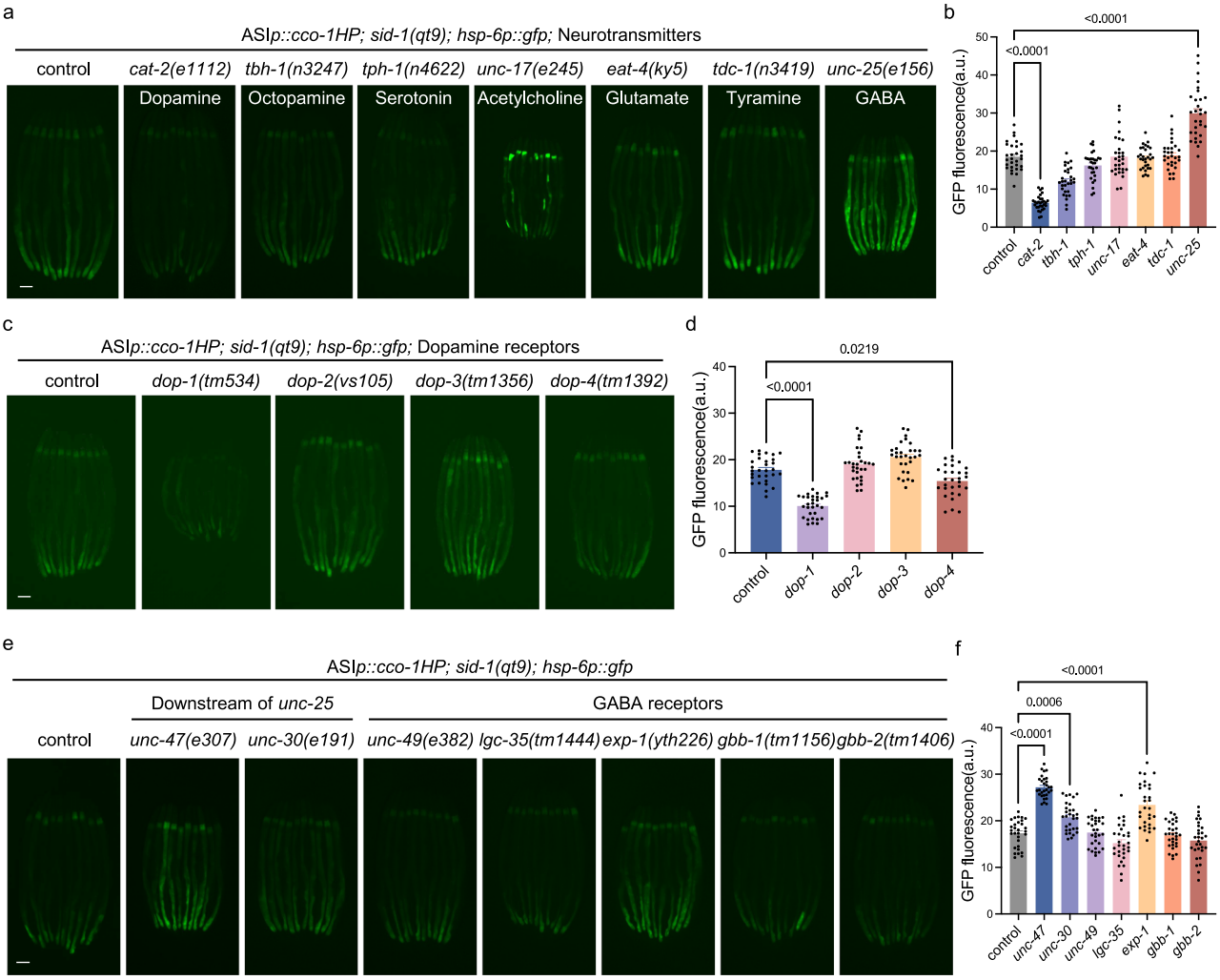


**Fig. 5 | The UPR$^{mt}$ induced by ASI *cco-1* KD is mediated by Dopamine and negatively regulated by GABA. a** Representative fluorescence photomicrographs of *hsp-6p::gfp* in wild-type, *cat-2, tbh-1, tph-1, unc-17, eat-4, tdc-1* and *unc-25* animals in *gpa-4p::cco-1HP* background. **b** Fluorescence intensities of *hsp-6p::gfp* in animals shown in (**a**) were quantified using ImageJ. n = 30 worms. **c** Representative fluorescence photomicrographs of *hsp-6p::gfp* in wild-type, *dop-1, dop-2, dop-3* and *dop-4* in *gpa-4p::cco-1HP* background. **d** Fluorescence intensities of *hsp-6p::gfp* in animals shown in (**c**) were quantified using ImageJ. n = 30 worms. **e** Representative fluorescence photomicrographs of *hsp-6p::gfp* in wild-type, *unc-47, unc-30, unc-49, lgc-35, exp-1, gbb-1* and *gbb-2* animals in *gpa-4p::cco-1HP* background. **f** Fluorescence intensities of *hsp-6p::gfp* in animals shown in (**e**) were quantified using ImageJ. n = 30 worms. *p* values were annotated via ordinary one-way ANOVA in (**b**), (**d**) and (**f**). Error bars, SEM. Scale bar, 100 µm. Source data are provided as a Source Data file. See also Supplementary Fig. 5.

pathways such as IIS and TGF-β[32,74–77]. Considering the close relationship among lipid metabolism, longevity and immune responses[78–81], we measured lipids levels using Oil Red O staining, which stains neutral triglycerides and lipids[82,83]. Both ASI *cco-1* KD and pan-neuronal *cco-1* KD animals had significantly lower lipid levels compared to control animals (Fig. 6g, h and Supplementary Fig. 6h, i). To investigate which fat metabolic pathways were affected by ASI-mitochondrial stress, we performed qPCR analyses to examine the expression of genes involved in lipid metabolism. *cpt-4*, a homolog of CPT1 (carnitine palmitoyl transferase) responsible for translocating fatty acids from the cytosol to the mitochondrial matrix during fatty acid β-oxidation[84,85], was significantly increased in both ASI *cco-1* KD and pan-neuronal *cco-1* KD background, while other lipid metabolism genes were not significantly affected (Fig. 6i and Supplementary Fig. 6j). This phenotype was confirmed using the *cpt-4p::gfp* reporter (Supplementary Fig. 6k, l).

The decreased fat storage was not dependent on known mitokine regulators including *egl-20, unc-31, unc-13, flp-2*, or *srz-75* (Supplementary Fig. 6h, i). *daf-7* is required for the lipid depletion in ASI *cco-1* KD animals (Fig. 6g, h). Additionally, the elevated transcription level of *cpt-4* in ASI *cco-1* KD animals was abolished by the *daf-7* mutation (Fig. 6i). Notably, both *daf-7* and *daf-1* mutation completely suppressed the reduced fat storage in ASI *cco-1* KD and pan-neuronal *cco-1* knockdown animals, which is restored by *daf-7p::daf-7* or RIM*p::daf-1* rescue (Fig. 6j, k). These results suggest that neuronal mitochondrial perturbation reduces body fat storage via the ASI-RIM axis and TGF-β signaling.

In summary, our study revealed that targeted mitochondrial stress in ASI neurons leads to systemic UPR$^{mt}$ activation and subsequent alterations in various physiological characteristics of the animals, highlight the complex interplay between mitochondrial function, TGF-β signaling, and organismal physiology.

## Discussion

In this study, we discovered that the TGF-β/DAF-7 signaling pathway in the ASI-RIM modulates the organism's response to pan-neuronal mitochondrial stress, transmitting this stress to the intestine, which induces UPR$^{mt}$ responses, altering lipid metabolic status, and influences aging. Specifically, perturbing mitochondrial function solely in ASI neurons is sufficient to induce cell non-autonomous UPR$^{mt}$, extend lifespan, and enhance pathogen resistance. The GABA

https://doi.org/10.1038/s41467-024-53093-9

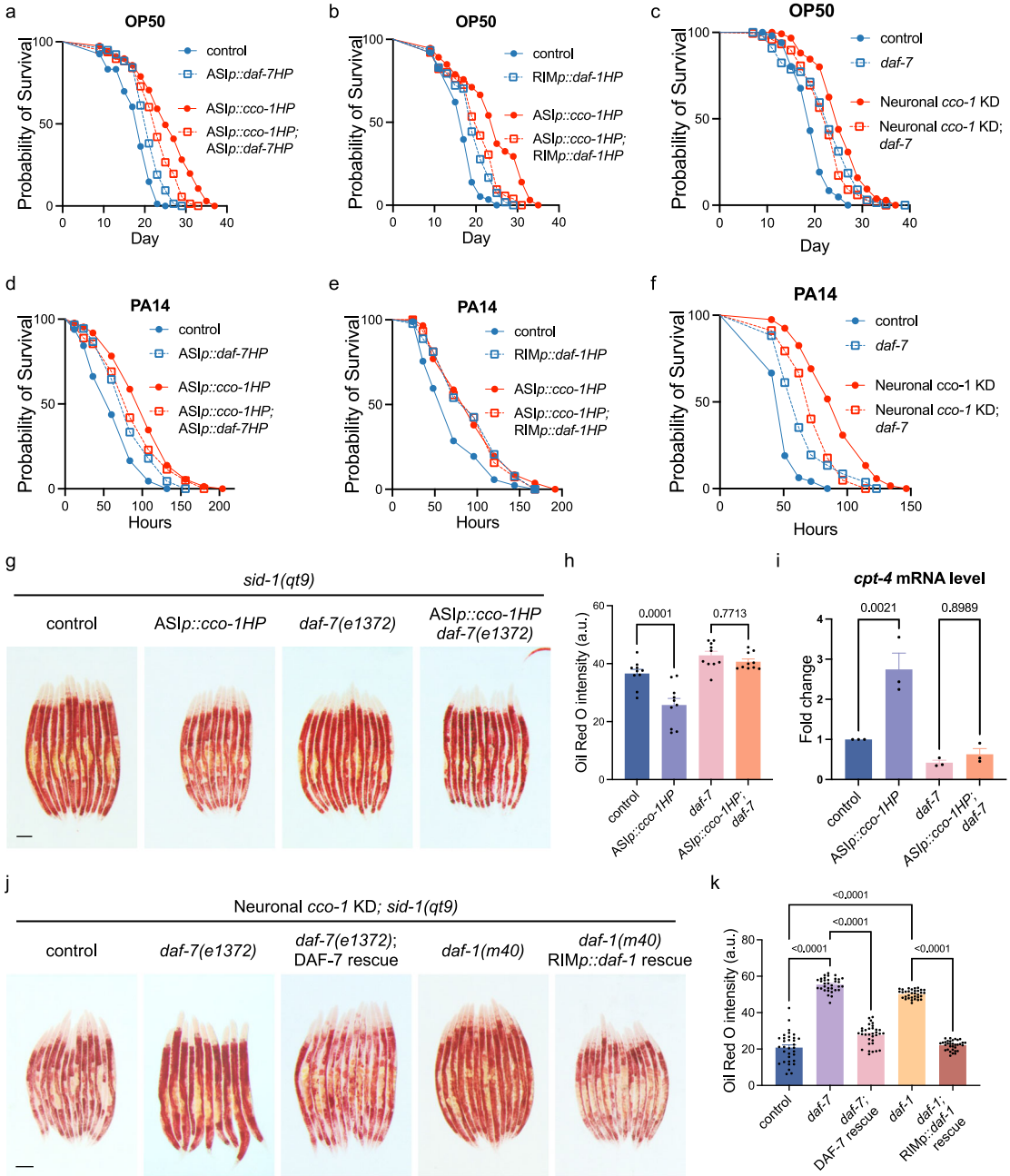


**Fig. 6 | Mitochondrial perturbation in ASI neurons alters various physiological characteristics of animals. a** Lifespan analysis of *gpa-4p::cco-1HP* animals with or without *gpa-4p::daf-7HP*. **b** Lifespan analysis of *gpa-4p::cco-1HP* animals with or without *F23H12.7p::daf-1HP*. **c** Lifespan analysis of neuronal *cco-1* knockdown animals with or without *daf-7* mutation. **d** Survival analysis of *gpa-4p::cco-1HP* animals with or without *gpa-4p::daf-7HP* feeding with *P. aeruginosa*. **e** Survival analysis of *gpa-4p::cco-1HP* animals with or without *F23H12.7p::daf-1HP* feeding with *P. aeruginosa*. **f** Survival analysis of neuronal *cco-1* knockdown animals with or without *daf-7* mutation feeding with *P. aeruginosa*. **g** Representative photomicrographs of Oil red O staining of control and *gpa-4p::cco-1HP* animals with or without *daf-7* mutation. **h** Intensities of Oil red O staining signals in the entire intestine of animals shown in (**g**) were quantified using ImageJ. n = 10 worms. **i** Relative mRNA level of *cpt-4* in control and *gpa-4p::cco-1HP* animals with or without *daf-7* mutation. n = 3 biological replicates. **j** Representative photomicrographs of Oil red O staining of neuronal *cco-1* knockdown animals with or without *daf-7* or *daf-1* mutation and the expression of *daf-7p::daf-7(cDNA)* or *F23H12.7p::daf-1(cDNA)*. **k** Intensities of Oil red O staining signals in the entire intestine of animals shown in (**j**) were quantified using ImageJ. n = 33 worms. *p* values were annotated via ordinary one-way ANOVA in (**h**), (**i**) and (**k**). Error bars, SEM. Lifespan and survival analysis have been repeated at least two times. Scale bar, 100 μm. Source data are provided as a Source Data file.See also Supplementary Fig. 6 and Supplementary Table 1.

suppresses systemic UPR$^{mt}$ activation in response to ASI-specific mitochondrial stress, while dopamine is necessary for this activation. Together, our findings highlight a central role for TGF-β/DAF-7 in regulating the systemic mitochondrial stress response and various physiological characteristics via the ASI-RIM axis (Fig. 7).

Morphogens serve as key signaling molecules in inter-tissue and inter-cell communication by establishing concentration gradients across tissues, ensuring that the entire organism adapts to stress in a coordinated manner[86,87]. The identification of Wnt as the initial morphogen functioning as a "mitokine" signal, orchestrating systemic mitochondrial stress adaptation, and influencing the aging process

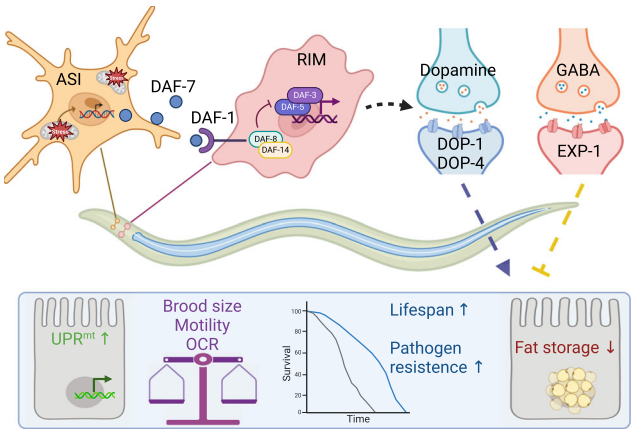


**Fig. 7 | Schematic model of ASI-RIM neuron axis coordinating the systemic mitochondrial stress response via TGF-β/DAF-7 signaling.** Neuronal mitochondrial stress initiated a TGF-β signaling cascade of ASI sensory neurons and RIM interneurons axis that ensure cell non-autonomous UPR$^{mt}$ induction in peripheral tissues. ASI-specific neuronal mitochondrial stress induced cell non-autonomous UPR$^{mt}$ which was mediated by dopamine and negatively regulated by GABA, confer increased lifespan, enhanced pathogen tolerance, fat storage depletion, and various physiological changes. Created in BioRender. Wang, Z. (2023) BioRender.com/h64v432.

invites speculation about the broader role of morphogens as crucial signaling molecules in inter-tissue and inter-cell communication[11,26,88,89]. In this study, we further identified a crucial morphogen, TGF-β, in the regulation of inter-tissue mitochondrial stress communication. Previous studies suggest that TGF-β exhibits dual roles in mitochondrial function: it can impair mitochondrial activity and elevate reactive oxygen species in certain conditions, such as idiopathic pulmonary fibrosis and tumor effusion[90–92], while also enhancing OXPHOS and ATP production in others, like metastatic breast cancer cells[93,94]. Interestingly, TGF-β signaling can mediate UPR$^{mt}$ and mitochondrial fission induced by extracellular matrix remodeling in human cells[95]. These findings align with the evolving understanding of morphogens, which are traditionally seen as key contributors to developmental processes. It highlights their significant role as regulators in mitochondrial adaptive responses, particularly in the context of aging and pathological processes.

It is important to note that TGF-β plays distinct roles in various stress responses. In our study, the loss of TGF-β/*daf-7* suppressed cell non-autonomous UPR$^{mt}$ activation. In contrast, *daf-7* mutants further enhanced cell non-autonomous UPR$^{ER}$ in a neuronal *xbp-1s* expression background. This aligns with previous findings showing that intestinal UPR$^{ER}$ activation is further increased in *daf-7* mutants in response to neuronal *xbp-1s* overexpression[96]. Additionally, *daf-7* is required for transforming environmental 1-undecene odor signal to RIM/RIC neurons for cell non-autonomous UPR$^{ER}$ regulation[97]. While TGF-β/*daf-7* signaling appears to suppress UPR$^{mt}$ activation under mitochondrial stress, it paradoxically enhances UPR$^{ER}$ under ER stress induced by neuronal *xbp-1s* overexpression. These findings suggest a complex regulatory mechanism where TGF-β signaling modulates different stress pathways in a context-dependent manner.

Neuronal coordination of systemic mitochondrial stress responses plays a fundamental role in organismal metabolism and aging[98]. Mitochondria are crucial for lipid metabolism, particularly fatty acid β-oxidation, which helps regulate fat storage and is associated with metabolic disorders and obesity[99]. Lipid metabolism is also interconnected with aging[78,79] and is essential for immune activation and pathogen defense[80,81]. In this study, we observed that manipulating mitochondrial function in just one pair of ASI sensory neurons is sufficient to induce fat depletion via activation of β-oxidation in distal tissues. This indicates broader physiological alterations in response to ASI-mitochondrial perturbations. This finding suggests that targeting sensory inputs or corresponding receptors in specific sensory neurons could be a promising approach to maintaining mitochondrial homeostasis and balancing fat storage levels.

The nervous system's complexity often involves multiple signals acting antagonistically on a particular phenotype. In *C. elegans*, dopamine and GABA exemplify this by regulating the egg-laying rate. Our study adds to this understanding by revealing that UPR$^{mt}$ activated by ASI-specific mitochondrial dysfunction is positively regulated by dopamine but negatively regulated by GABA. Moreover, the systemic activation of UPR$^{mt}$ induced by the loss of GABA also requires TGF-β/DAF-7 but is only partially dependent on dopamine. This suggests a complex interaction between GABA, dopamine, and TGF-β in regulating UPR$^{mt}$. Ultimately, the output of neuronal coordination of mitochondrial stress response is the balanced result of both suppression and activation signals, highlighting the intricate interplay within the nervous system to control organismal-wide stress response.

## Methods

### Caenorhabditis elegans maintenance

Studies were undertaken with *C. elegans* hermaphrodites. If needed, nematode males are obtained by heat shock. Nematodes were maintained and experimentally examined at 20°C on standard nematode growth medium agar plates seeded with *Escherichia coli* OP50, unless otherwise indicated. See all strains used or generated in Supplementary Table 2.

### Transgenic strain construction

KOD-Plus-Neo (TOYOBO Cat#KOD-401) and KOD-Plus-Mutagenesis Kit (TOYOBO Cat#SMK-101) was used for PCR, ClonExpress Ultra One Step Cloning Kit (Vazyme Cat#C115-02) and Trelief® Seamless Cloning Kit (TSINGKE Cat#TSV-S3) was used for recombination.

Transgenic strains were generated by microinjecting target constructs (5–100 ng/μL) mixed with a pRF4(*rol-6*) (60 ng/μL), *myo-3p::DsRed* (25 ng/μL), *odr-1p::RFP* (50 ng/μL), *unc-122p::RFP* (50 ng/μL) co-injection maker. Integrated lines were generated using UV irradiation and outcrossed six times with control animals. The original plasmid backbone is pNB23 with the 5'utr region of *unc-54*. More detail information of the plasmids were listed in Supplementary Table 2.

### RNAi feeding

Synchronized worms were bleached and grown from hatch on *Escherichia coli* HT115 strains containing an empty vector control or double-stranded RNA targeting to different genes. RNAi strains were from the Vidal library if present, or the Ahringer library if absent in the Vidal library.

### CRISPR/Cas9 mediated gene editing

To generate *exp-1(yth226)* mutants, two single-guide RNA (sgRNA) targeting sequence (5'-TGAACCACTTGGACGGGGAG-3', 5'-ACTGAACACTGATTCCGTAT-3') of *exp-1* were used. The CRISPR/Cas9 technology in accordance with published protocols[100]. The sgRNA vectors (40 ng/μL), the Cas9 vector (40 ng/μL) and the co-injection marker Rol-6 (80 ng/μL) were injected. Roller F1 worms were singled into new plates and examined by PCR amplification and sequencing. 2 x Rapid Taq Master Mix (Vazyme Cat#P222-03) was used for PCR, MinElute PCR Purification Kit (Qiagen Cat#28004) was used for DNA purification and QlAprep Spin Miniprep Kit (Qiagen Cat#27104) was used for plasmid extraction.

### Imaging and analysis of the fluorescence intensity

For fluorescence image, worms were anesthetized with 50 mM sodium azide as soon as possible, and photographs were taken in no more than 5 min using a Leica M165 FC dissecting microscope and LAS X software

3.3 (Leica). Micrographs of specific neurons colocalization images were taken using a Zeiss Imager M2 microscope and ZEN (Zeiss) software. Fluorescent *daf-7* and *daf-1* expression images were taken using a Leica TCS SP8 microscope and LAS X software. Exposure times were the same within each experiment. To quantify the fluorescent intensity of each UPR reporters, the entire intestine regions were outlined and quantified using ImageJ 1.53k (Wayne Rasband (NIH)) software. To quantify *daf-7p::gfp* fluorescent intensity, each ASI neuron body were outlined and quantified using ImageJ. To quantify *cpt-4p::gfp* fluorescent intensity, the whole worm were outlined and quantified using ImageJ.

### RNA isolation and quantitative PCR analyses

Total RNA was isolated using TRIzol (Invitrogen Cat#15596026). Worms were synchronized and washed off the plates using M9 buffer, and 1 mL TRIzol were added to the samples and homogenized by repeated freezing and thawing using liquid nitrogen for 6 times. RNA was isolated according to manufacturer's instructions. DNA was wiped off and cDNA was synthesized using the ReverTra Ace® qPCR RT Master Mix with gDNA remover (Toyobo Cat#FSQ-301). Gene expression levels were determined by real-time PCR using SYBR Green Realtime PCR Master Mix (Toyobo Cat#QPK-201) and Bio-rad CFX96/384 Real-Time PCR Detection Systems. Relative gene expression was normalized to *act-3* (*T04C12.4*) or *act-1* (T04C12.6) mRNA levels. Fold changes in gene expression were calculated using the comparative $\Delta\Delta C_t$ method, and then normalized to the control for every single biological repeat. The primer sequences used in the quantitative PCR are shown in Supplementary Table 3.

### Lifespan analysis

Lifespan experiments were performed on NGM plates at 20 °C as previously described[101]. While temperature shift experiments, synchronized eggs were seeded at 20 °C and then transferred to 25 °C at the L4 stage. To prevent progeny production, 150 μL 10 mg/mL 5-fluoro-20-deoxyuridine (FUdR (Aladdin Cat#F110732)) was added to seeded plates. Worms were synchronized by bleach and were grown on OP50 from hatch, and transited to FUdR plates from day 1 of adulthood, then transferred a second time at day 5 of adulthood. Animals were counted every second day and were scored as dead if they failed to respond when touched. Prism 10.2.3 software (GraphPad Software) was used for statistical analysis. Log-rank (Mantel-Cox) method was used to determine the significance difference. All survival data are available in Supplementary Table 1.

### *P. aeruginosa* slow-killing assay

Slow-killing experiments were performed as previously described[102]. *P. aeruginosa* was cultured overnight in LB containing 50 μg/ml kanamycin at 37 C and then seeded onto slow-killing nematode growth medium (NGM) agar plates (with 0.35% peptone). Plates were allowed to dry at room temperature, incubated at 37 °C for 24 h and then balanced at room temperature for another 24 h. 100 μl 10 mg/ml FUdR was added in the slow-killing plates. Synchronized day 1 worms were transferred from *E. coli* NGM plates to slow-killing plates and maintained at 25 °C. Animals were counted at the described times and were scored as dead if they failed to respond when touched. Prism 10.2.3 software was used for statistical analysis. Log-rank (Mantel-Cox) method was used to determine the significance difference. Each experiment was repeated at least two times. All original data are available in Supplementary Table 1.

### Brood size assay

At least 10 synchronized L4 worms were placed onto NGM plates with seeded OP50 at 20 °C and transferred to fresh NGM plates every day until they stopped laying eggs. The total number of progenies was counted for each strain. Each experiment was repeated for three times.

### Developmental rate assay

Worms were synchronized and about 300 eggs of each strain were placed onto NGM plates with seeded OP50. These worms grow at 17.5 °C for 108 h and the number of worms at each developmental stage was calculated.

### Motility assay

For bending ability test, day 1 worms were transferred to a drop of M9 buffer. After 1 min of adaptation, the number of body bends during 20 s was counted. A body bend was defined as change in the direction of bending in the middle of the body[103].

For crawling ability test, day 1 worms were transferred to an empty NGM plate without OP50. After 1 min of adaptation, 20 s of crawling movies were captured via Wormaction1858 (Zebra Scientific Development) software, and the center point speed was analyzed via WormLab (MBF Bioscience) software.

### Measurement of oxygen consumption rate

Oxygen consumption rate (OCR) was measured using a Seahorse XFe96 analyzer (Seahorse Bioscience) at 20 °C as described previously[104]. Fifteen synchronized D1 worms of each strain were transferred into each well of a 96-well microplate containing 200 μL M9, 5 wells per strain. Basal respiration was measured for a total of 90 min, in 9 min intervals that included a 3 min mix, a 3 min time delay and a 3 min measurement. Experiments were repeated at least three times for each strain.

### Oil-red-O staining and quantification

The Oil-Red-O (ORO) staining was performed as previously described[105]. Briefly, synchronized day 1 worms were collected and washed three times with M9 + 0.1% Triton X-100 (Sigma Cat#T8787). Worms were suspended in 100 μL M9, and then fix worms by adding 100 μL 4% paraformaldehyde (PFA). After 1 h incubating, wash worms with M9 + 0.1% Triton X-100 3 times to remove PFA and resuspension in 1 mL 60% isopropanol to dehydrate. Worms were then incubated with rocking in 500 μL 60% ORO solution (Abcam Cat#ab146295, 0.5 g/100 mL isopropanol stock solution, freshly dilute with $ddH_2O$, rock for several hours and filter with a 0.45-μm filter) for 2.5 h at 20 °C. Stained worms were washed with M9 + 0.1% Triton X-100 3 times, and then imaged using a Leica M165 FC dissecting microscope. To quantify ORO signals, the channels of images were split and the mean intensity in the red color channel of the post pharyngeal intestine was measured using Image J software.

### Statistical analysis

The statistical analyses were performed using GraphPad Prism 10.2.3. Statistical significance was calculated by unpaired t-test, ordinary one-way ANOVA and two-way ANOVA as annotated. The data were presented as the means ± SEM with indicated *p* values.

### Reporting summary

Further information on research design is available in the Nature Portfolio Reporting Summary linked to this article.

## Data availability

Additional data related to this paper may be requested from authors. All strains synthesized in this manuscript are derivatives of N2 or other strains from CGC and are either made available on CGC or available upon request. Source data are provided with this paper.

## References

1. Singh, J. & Aballay, A. Neural control of behavioral and molecular defenses in *C. elegans*. *Curr. Opin. Neurobiol.* **62**, 34–40 (2020).
2. Srinivasan, S. Regulation of body fat in *Caenorhabditis elegans*. *Annu Rev. Physiol.* **77**, 161–178 (2015).

3. Durieux, J., Wolff, S. & Dillin, A. The cell-non-autonomous nature of electron transport chain-mediated longevity. *Cell* **144**, 79–91 (2011).
4. Shao, L. W., Niu, R. & Liu, Y. Neuropeptide signals cell non-autonomous mitochondrial unfolded protein response. *Cell Res* **26**, 1182–1196 (2016).
5. Berendzen, K. M. et al. Neuroendocrine coordination of mitochondrial stress signaling and proteostasis. *Cell* **166**, 1553–1563.e1510 (2016).
6. Shen, K. et al. The germline coordinates mitokine signaling. *Cell* **187**, 4605–4620.e4617 (2024).
7. Chen, L. T. et al. Neuronal mitochondrial dynamics coordinate systemic mitochondrial morphology and stress response to confer pathogen resistance in *C. elegans*. *Dev. Cell* **56**, 1770–1785.e1712 (2021).
8. Dishart, J. G. et al. Olfaction regulates peripheral mitophagy and mitochondrial function. *Sci. Adv.* **10**, eadn0014 (2024).
9. Kang, G. M. et al. Mitohormesis in hypothalamic POMC neurons mediates regular exercise-induced high-turnover metabolism. *Cell Metab.* **33**, 334–349.e336 (2021).
10. Gomez-Valades, A. G. et al. Mitochondrial cristae-remodeling protein OPA1 in POMC neurons couples Ca(2+) homeostasis with adipose tissue lipolysis. *Cell Metab.* **33**, 1820–1835.e1829 (2021).
11. Zhang, Q. et al. The mitochondrial unfolded protein response is mediated cell-non-autonomously by retromer-dependent Wnt signaling. *Cell* **174**, 870–883 (2018).
12. Liu, Y. et al. Two sensory neurons coordinate the systemic mitochondrial stress response via GPCR signaling in *C. elegans*. *Dev. Cell* **57**, 2469–2482.e2465 (2022).
13. Cheruku, H. R. et al. Transforming growth factor-β, MAPK and Wnt signaling interactions in colorectal cancer. *EuPA Open Proteom.* **8**, 104–115 (2015).
14. Zhu, T. et al. The S100 calcium binding protein A11 promotes liver fibrogenesis by targeting TGF-beta signaling. *J. Genet Genomics* **49**, 338–349 (2022).
15. Yousefi, F. et al. TGF-beta and WNT signaling pathways in cardiac fibrosis: Non-coding RNAs come into focus. *Cell Commun. Signal* **18**, 87 (2020).
16. Dzialo, E., Tkacz, K. & Blyszczuk, P. Crosstalk between the TGF-beta and WNT signalling pathways during cardiac fibrogenesis. *Acta Biochim Pol.* **65**, 341–349 (2018).
17. Zhang, K., Zhang, M., Luo, Z., Wen, Z. & Yan, X. The dichotomous role of TGF-beta in controlling liver cancer cell survival and proliferation. *J. Genet Genomics* **47**, 497–512 (2020).
18. Ren, P. et al. Control of *C. elegans* larval development by neuronal expression of a TGF-beta homolog. *Science* **274**, 1389–1391 (1996).
19. Gallagher, T., Kim, J., Oldenbroek, M., Kerr, R. & You, Y. J. ASI regulates satiety quiescence in *C. elegans*. *J. Neurosci.* **33**, 9716–9724 (2013).
20. Meisel, J. D., Panda, O., Mahanti, P., Schroeder, F. C. & Kim, D. H. Chemosensation of bacterial secondary metabolites modulates neuroendocrine signaling and behavior of *C. elegans*. *Cell* **159**, 267–280 (2014).
21. Moore, R. S., Kaletsky, R. & Murphy, C. T. Piwi/PRG-1 argonaute and TGF-beta mediate transgenerational learned pathogenic avoidance. *Cell* **177**, 1827–1841 (2019).
22. Greer, E. R., Perez, C. L., Van Gilst, M. R., Lee, B. H. & Ashrafi, K. Neural and molecular dissection of a *C. elegans* sensory circuit that regulates fat and feeding. *Cell Metab.* **8**, 118–131 (2008).
23. You, Y. J., Kim, J., Raizen, D. M. & Avery, L. Insulin, cGMP, and TGF-beta signals regulate food intake and quiescence in *C. elegans*: a model for satiety. *Cell Metab.* **7**, 249–257 (2008).
24. Wexler, L. R., Miller, R. M. & Portman, D. S. *C. elegans* males integrate food signals and biological sex to modulate state-dependent chemosensation and behavioral prioritization. *Curr. Biol.* **30**, 2695–2706.e2694 (2020).
25. Morita, K., Chow, K. L. & Ueno, N. Regulation of body length and male tail ray pattern formation of *Caenorhabditis elegans* by a member of TGF-beta family. *Development* **126**, 1337–1347 (1999).
26. Zhang, Q. et al. The memory of neuronal mitochondrial stress is inherited transgenerationally via elevated mitochondrial DNA levels. *Nat. Cell Biol.* **23**, 870–880 (2021).
27. Krishna, S., Maduzia, L. L. & Padgett, R. W. Specificity of TGFbeta signaling is conferred by distinct type I receptors and their associated SMAD proteins in *Caenorhabditis elegans*. *Development* **126**, 251–260 (1999).
28. Ron, D. & Walter, P. Signal integration in the endoplasmic reticulum unfolded protein response. *Nat. Rev. Mol. Cell Biol.* **8**, 519–529 (2007).
29. Taylor, R. C. & Dillin, A. XBP-1 is a cell-nonautonomous regulator of stress resistance and longevity. *Cell* **153**, 1435–1447 (2013).
30. Douglas, P. M. et al. Heterotypic signals from neural HSF-1 separate thermotolerance from longevity. *Cell Rep.* **12**, 1196–1204 (2015).
31. Link, C. D., Cypser, J. R., Johnson, C. J. & Johnson, T. E. Direct observation of stress response in *Caenorhabditis elegans* using a reporter transgene. *Cell Stress Chaperones* **4**, 235–242 (1999).
32. Schackwitz, W. S., Inoue, T. & Thomas, J. H. Chemosensory neurons function in parallel to mediate a pheromone response in *C. elegans*. *Neuron* **17**, 719–728 (1996).
33. Hammarlund, M., Hobert, O., Miller, D. M. 3rd & Sestan, N. The CeNGEN project: The complete gene expression map of an entire nervous system. *Neuron* **99**, 430–433 (2018).
34. Taylor, S. R. et al. Molecular topography of an entire nervous system. *Cell* **184**, 4329–4347 (2021).
35. Barrett, A. et al. A head-to-head comparison of ribodepletion and polyA selection approaches for *Caenorhabditis elegans* low input RNA-sequencing libraries. *G3 (Bethesda)* 11, jkab121 (2021).
36. Jansen, G. et al. The complete family of genes encoding G proteins of *Caenorhabditis elegans*. *Nat. Genet* **21**, 414–419 (1999).
37. Tobin, D. M. et al. Combinatorial expression of TRPV channel proteins defines their sensory functions and subcellular localization in *C. elegans* neurons. *Neuron* **35**, 307–318 (2002).
38. Flames, N. & Hobert, O. Gene regulatory logic of dopamine neuron differentiation. *Nature* **458**, 885–889 (2009).
39. Ortiz, C. O. et al. Searching for neuronal left/right asymmetry: genomewide analysis of nematode receptor-type guanylyl cyclases. *Genetics* **173**, 131–149 (2006).
40. Sengupta, P., Chou, J. H. & Bargmann, C. I. *odr-10* encodes a seven transmembrane domain olfactory receptor required for responses to the odorant diacetyl. *Cell* **84**, 899–909 (1996).
41. Miranda-Vizuete, A. et al. Lifespan decrease in a *Caenorhabditis elegans* mutant lacking TRX-1, a thioredoxin expressed in ASJ sensory neurons. *FEBS Lett.* **580**, 484–490 (2006).
42. Georgi, L. L., Albert, P. S. & Riddle, D. L. *daf-1*, a *C. elegans* gene controlling Dauer larva development, encodes a novel receptor protein kinase. *Cell* **61**, 635–645 (1990).
43. Estevez, M. et al. The *daf-4* gene encodes a bone morphogenetic protein receptor controlling *C. elegans* Dauer larva development. *Nature* **365**, 644–649 (1993).
44. Shaw, W. M., Luo, S., Landis, J., Ashraf, J. & Murphy, C. T. The *C. elegans* TGF-beta Dauer pathway regulates longevity via insulin signaling. *Curr. Biol.* **17**, 1635–1645 (2007).
45. Inoue, T. & Thomas, J. H. Targets of TGF-beta signaling in *Caenorhabditis elegans* Dauer formation. *Dev. Biol.* **217**, 192–204 (2000).
46. Thomas, J. H., Birnby, D. A. & Vowels, J. J. Evidence for parallel processing of sensory information controlling dauer formation in *Caenorhabditis elegans*. *Genetics* **134**, 1105–1117 (1993).

47. da Graca, L. S. et al. DAF-5 is a Ski oncoprotein homolog that functions in a neuronal TGF beta pathway to regulate *C. elegans* Dauer development. *Development* **131**, 435–446 (2004).
48. Patterson, G. I., Koweek, A., Wong, A., Liu, Y. & Ruvkun, G. The DAF-3 Smad protein antagonizes TGF-beta-related receptor signaling in the *Caenorhabditis elegans* Dauer pathway. *Genes Dev.* **11**, 2679–2690 (1997).
49. Tewari, M. et al. Systematic interactome mapping and genetic perturbation analysis of a *C. elegans* TGF-beta signaling network. *Mol. Cell* **13**, 469–482 (2004).
50. Riddle D. L., Albert P. S. Genetic and environmental regulation of Dauer larva development. In: *C. elegans II* (eds Riddle D. L., Blumenthal T., Meyer B. J., Priess J. R.). 2nd edn (1997).
51. Alkema, M. J., Hunter-Ensor, M., Ringstad, N. & Horvitz, H. R. Tyramine functions independently of octopamine in the *Caenorhabditis elegans* nervous system. *Neuron* **46**, 247–260 (2005).
52. Brockie, P. J., Madsen, D. M., Zheng, Y., Mellem, J. & Maricq, A. V. Differential expression of glutamate receptor subunits in the nervous system of *Caenorhabditis elegans* and their regulation by the homeodomain protein UNC-42. *J. Neurosci.* **21**, 1510–1522 (2001).
53. Collet, J., Spike, C. A., Lundquist, E. A., Shaw, J. E. & Herman, R. K. Analysis of *osm-6*, a gene that affects sensory cilium structure and sensory neuron function in *Caenorhabditis elegans*. *Genetics* **148**, 187–200 (1998).
54. Much, J. W., Slade, D. J., Klampert, K., Garriga, G. & Wightman, B. The fax-1 nuclear hormone receptor regulates axon pathfinding and neurotransmitter expression. *Development* **127**, 703–712 (2000).
55. Schiffer, J. A. et al. *Caenorhabditis elegans* processes sensory information to choose between freeloading and self-defense strategies. *eLife* **9**, e56186 (2020).
56. Park, D., Estevez, A. & Riddle, D. L. Antagonistic Smad transcription factors control the Dauer/non-Dauer switch in *C. elegans*. *Development* **137**, 477–485 (2010).
57. Park, D. et al. Repression of a potassium channel by nuclear hormone receptor and TGF-beta signaling modulates insulin signaling in *Caenorhabditis elegans*. *PLoS Genet* **8**, e1002519 (2012).
58. Li, X. et al. Protein disulfide isomerase PDI-6 regulates Wnt secretion to coordinate inter-tissue UPR(mt) activation and lifespan extension in *C. elegans*. *Cell Rep.* **39**, 110931 (2022).
59. Tian, Y. et al. Mitochondrial stress induces chromatin reorganization to promote longevity and UPR(mt). *Cell* **165**, 1197–1208 (2016).
60. Zhu, D. et al. NuRD mediates mitochondrial stress-induced longevity via chromatin remodeling in response to acetyl-CoA level. *Sci. Adv.* **6**, eabb2529 (2020).
61. Madison, J. M., Nurrish, S. & Kaplan, J. M. UNC-13 interaction with syntaxin is required for synaptic transmission. *Curr. Biol.* **15**, 2236–2242 (2005).
62. Speese, S. et al. UNC-31 (CAPS) is required for dense-core vesicle but not synaptic vesicle exocytosis in *Caenorhabditis elegans*. *J. Neurosci.* **27**, 6150–6162 (2007).
63. Jacob, T. C. & Kaplan, J. M. The EGL-21 carboxypeptidase *E facilitates* acetylcholine release at *Caenorhabditis elegans* neuromuscular junctions. *J. Neurosci.* **23**, 2122–2130 (2003).
64. Chase D. L., Koelle M. R. Biogenic amine neurotransmitters in *C. elegans*. *WormBook*, 1-15 (2007).
65. Suo, S., Sasagawa, N. & Ishiura, S. Cloning and characterization of a *Caenorhabditis elegans* D2-like dopamine receptor. *J. Neurochem* **86**, 869–878 (2003).
66. Eastman, C., Horvitz, H. R. & Jin, Y. Coordinated transcriptional regulation of the *unc-25* glutamic acid decarboxylase and the *unc-47* GABA vesicular transporter by the *Caenorhabditis elegans* UNC-30 homeodomain protein. *J. Neurosci.* **19**, 6225–6234 (1999).
67. McIntire, S. L., Reimer, R. J., Schuske, K., Edwards, R. H. & Jorgensen, E. M. Identification and characterization of the vesicular GABA transporter. *Nature* **389**, 870–876 (1997).
68. Jobson, M. A. et al. Spillover transmission is mediated by the excitatory GABA receptor LGC-35 in *C. elegans*. *J. Neurosci.* **35**, 2803–2816 (2015).
69. Beg, A. A. & Jorgensen, E. M. EXP-1 is an excitatory GABA-gated cation channel. *Nat. Neurosci.* **6**, 1145–1152 (2003).
70. Dittman, J. S. & Kaplan, J. M. Behavioral impact of neurotransmitter-activated G-protein-coupled receptors: muscarinic and GABAB receptors regulate *Caenorhabditis elegans* locomotion. *J. Neurosci.* **28**, 7104–7112 (2008).
71. Bamber, B. A., Beg, A. A., Twyman, R. E. & Jorgensen, E. M. The *Caenorhabditis elegans unc-49* locus encodes multiple subunits of a heteromultimeric GABA receptor. *J. Neurosci.* **19**, 5348–5359 (1999).
72. Tan, M. W., Mahajan-Miklos, S. & Ausubel, F. M. Killing of *Caenorhabditis elegans* by *Pseudomonas aeruginosa* used to model mammalian bacterial pathogenesis. *Proc. Natl Acad. Sci. USA* **96**, 715–720 (1999).
73. Pellegrino, M. W. et al. Mitochondrial UPR-regulated innate immunity provides resistance to pathogen infection. *Nature* **516**, 414–417 (2014).
74. Tataridas-Pallas, N. et al. Neuronal SKN-1B modulates nutritional signalling pathways and mitochondrial networks to control satiety. *PLoS Genet* **17**, e1009358 (2021).
75. Dixit, A. et al. Neuronal control of lipid metabolism by STR-2 G protein-coupled receptor promotes longevity in *Caenorhabditis elegans*. *Aging Cell* **19**, e13160 (2020).
76. An, L., Fu, X., Chen, J. & Ma, J. Application of *Caenorhabditis elegans* in lipid metabolism research. *Int J. Mol. Sci.* **24**, 1173 (2023).
77. Srinivasan, S. Neuroendocrine control of lipid metabolism: lessons from *C. elegans*. *J. Neurogenet.* **34**, 482–488 (2020).
78. Wang, M. C., O'Rourke, E. J. & Ruvkun, G. Fat metabolism links germline stem cells and longevity in *C. elegans*. *Science* **322**, 957–960 (2008).
79. Han, S. et al. Mono-unsaturated fatty acids link H3K4me3 modifiers to *C. elegans* lifespan. *Nature* **544**, 185–190 (2017).
80. Nandakumar, M. & Tan, M. W. Gamma-linolenic and stearidonic acids are required for basal immunity in *Caenorhabditis elegans* through their effects on *p38* MAP kinase activity. *PLoS Genet* **4**, e1000273 (2008).
81. Anderson, S. M. et al. The fatty acid oleate is required for innate immune activation and pathogen defense in *Caenorhabditis elegans*. *PLoS Pathog.* **15**, e1007893 (2019).
82. Soukas, A. A., Kane, E. A., Carr, C. E., Melo, J. A. & Ruvkun, G. Rictor/TORC2 regulates fat metabolism, feeding, growth, and life span in *Caenorhabditis elegans*. *Genes Dev.* **23**, 496–511 (2009).
83. O'Rourke, E. J., Soukas, A. A., Carr, C. E. & Ruvkun, G. *C. elegans* major fats are stored in vesicles distinct from lysosome-related organelles. *Cell Metab.* **10**, 430–435 (2009).
84. Dasgupta, M. et al. NHR-49 transcription factor regulates immunometabolic response and survival of *Caenorhabditis elegans* during *Enterococcus faecalis* infection. *Infect. Immun.* **88**, e00130–00120 (2020).
85. Lee, K., Kerner, J. & Hoppel, C. L. Mitochondrial carnitine palmitoyltransferase 1a (CPT1a) is part of an outer membrane fatty acid transfer complex. *J. Biol. Chem.* **286**, 25655–25662 (2011).
86. Zhang, Q., Wang, Z. & Tian, Y. Inter-tissue communication of mitochondrial stress in aging. *Yi Chuan* **45**, 187–197 (2023).
87. Li, J., Cui, J. & Tian, Y. Neuron-periphery mitochondrial stress communication in aging and diseases. *Life Med.* **1**, 168–178 (2022).
88. Zhang, H. et al. Inter-tissue communication of mitochondrial stress and metabolic health. *Life Metab.* **2**, 1–11 (2023).

89. Zhang, Q. & Tian, Y. Molecular insights into the transgenerational inheritance of stress memory. *J. Genet Genomics* **49**, 89–95 (2022).
90. Yoon, Y. S., Lee, J. H., Hwang, S. C., Choi, K. S. & Yoon, G. T. G. F. beta1 induces prolonged mitochondrial ROS generation through decreased complex IV activity with senescent arrest in Mv1Lu cells. *Oncogene* **24**, 1895–1903 (2005).
91. Dimeloe, S. et al. Tumor-derived TGF-beta inhibits mitochondrial respiration to suppress IFN-gamma production by human CD4(+) T cells. *Sci. Signal* **12**, eaav3334 (2019).
92. Zhang, N. et al. TGF-beta changes cyto/mito-ribosome balance to target respiratory chain complex V biogenesis in pulmonary fibrosis therapy. *Signal Transduct. Target. Ther.* **8**, 136 (2023).
93. Gabriel, S. S. et al. Transforming growth factor-beta-regulated mTOR activity preserves cellular metabolism to maintain long-term T cell responses in chronic infection. *Immunity* **54**, 1698–1714 (2021).
94. Liu, Q. Q. et al. TGF-beta1-induced epithelial-mesenchymal transition increases fatty acid oxidation and OXPHOS activity via the p-AMPK pathway in breast cancer cells. *Oncol. Rep.* **44**, 1206–1215 (2020).
95. Zhang, H. et al. The extracellular matrix integrates mitochondrial homeostasis. *Cell* **187**, 4289–4304 (2024).
96. Ozbey, N. P. et al. Tyramine acts downstream of neuronal XBP-1s to coordinate inter-tissue UPR(ER) activation and behavior in *C. elegans*. *Dev. Cell* **55**, 754–770.e756 (2020).
97. De-Souza, E. A., Thompson, M. A. & Taylor, R. C. Olfactory chemosensation extends lifespan through TGF-beta signaling and UPR activation. *Nat. Aging* **3**, 938–947 (2023).
98. Chen, P. X., Zhang, L., Chen, D. & Tian, Y. Mitochondrial stress and aging: Lessons from *C. elegans*. *Semin Cell Dev. Biol.* **154**, 69–76 (2024).
99. Littlejohn, N. K., Seban, N., Liu, C. C. & Srinivasan, S. A feedback loop governs the relationship between lipid metabolism and longevity. *eLife* **9**, e58815 (2020).
100. Waaijers, S. et al. CRISPR/Cas9-targeted mutagenesis in *Caenorhabditis elegans*. *Genetics* **195**, 1187–1191 (2013).
101. Dillin, A. et al. Rates of behavior and aging specified by mitochondrial function during development. *Science* **298**, 2398–2401 (2002).
102. Kirienko, N. V., Cezairliyan, B. O., Ausubel, F. M. & Powell, J. R. *Pseudomonas aeruginosa PA14* pathogenesis in *Caenorhabditis elegans*. *Methods Mol. Biol.* **1149**, 653–669 (2014).
103. Calculli, G. et al. Systemic regulation of mitochondria by germline proteostasis prevents protein aggregation in the soma of *C. elegans*. *Sci. Adv.* **7**, eabg3012 (2021).
104. Houtkooper, R. H. et al. Mitonuclear protein imbalance as a conserved longevity mechanism. *Nature* **497**, 451–457 (2013).
105. Ching, WangF. Y. TT. Oil Red O Staining for Lipid Content in *Caenorhabditis elegans*. *Bio Protoc.* **11**, e4124 (2021).

## Acknowledgements

We thank Tian lab members for the insightful discussions and Y. Liu for helping with strain maintenance. In this study, Y.T. is supported by the National Key R&D Program of China (2022YFA1303000), the Strategic Priority Research Program of the Chinese Academy of Sciences (XDB39000000), the National Natural Science Foundation of China (31930023, 32225025, 92254305, 32321004), the CAS Project for Young Scientists in Basic Research (YSBR-076). Q.Z. was supported by the China National Postdoctoral Program for Innovative Talents (BX2021356), the National Natural Science Foundation of China (32471212, 32200624) and the China Postdoctoral Science Foundation (2021M703474). Several *C. elegans* strains used in this work were provided by the Caenorhabditis Genetics Center (CGC), funded by the NIH P40OD010440. Several deletion worm strains were also provided by the Japanese National BioResource Project.

## Author contributions

Y.T., Z.W., and Q.Z. conceived the study and wrote the manuscript. Z.W. performed the *C. elegans* crosses and strain generations. Z.W. performed fluorescence microscopy, RNAi, qPCR, *P. aeruginosa* slow-killing, motility, and oxygen consumption rate experiments. Z.W. and Q.Z. performed the Oil-Red-O staining, and life-span experiments. Z.W. and Y.J. performed plasmids construction and microinjection. Z.W., Q.Z. and J.Z. performed the brood size and developmental rate experiments.

## Competing interests

The authors declare no competing interests.

## Additional information

**Supplementary information** The online version contains supplementary material available at https://doi.org/10.1038/s41467-024-53093-9.

**Correspondence** and requests for materials should be addressed to Ye Tian.

**Peer review information** *Nature Communications* thanks the anonymous reviewers for their contribution to the peer review of this work. A peer review file is available.